J|A|C|S
ARTICLES
Published on Web 02/16/2006

Diastereoselective DNA Cleavage Recognition by Ni(II)•Gly-Gly-His-Derived Metallopeptides

Ya-Yin Fang,[†,§] Craig A. Claussen,[§] Kenny B. Lipkowitz,[‡] and Eric C. Long*[,§]

Contribution from the Department of Chemistry & Chemical Biology, Purdue School of Science, Indiana University—Purdue University Indianapolis (IUPUI), Indianapolis, Indiana 46202-3274, and Department of Chemistry, Howard University, Washington, D.C. 20059

Received October 12, 2005; E-mail: long@chem.iupui.edu

Abstract: Site-selective DNA cleavage by diastereoisomers of Ni(II)•Gly-Gly-His-derived metallopeptides was investigated through high-resolution gel analyses and molecular dynamics simulations. Ni(II)•L-Arg-Gly-His and Ni(II)•D-Arg-Gly-His (and their respective Lys analogues) targeted A/T-rich regions; however, the L-isomers consistently modified a subset of available nucleotides within a given minor groove site, while the D-isomers differed in both their sites of preference and their ability to target individual nucleotides within some sites. In comparison, Ni(II)•L-Pro-Gly-His and Ni(II)•D-Pro-Gly-His were unable to exhibit a similar diastereoselectivity. Simulations of the above systems, along with Ni(II)•Gly-Gly-His, indicated that the stereochemistry of the amino-terminal amino acid produces either an isohelical metallopeptide that associates stably at individual DNA sites (L-Arg or L-Lys) or, with D-Arg and D-Lys, a noncomplementary metallopeptide structure that cannot fully employ its side chain nor amino-terminal amine as positional stabilizing moieties. In contrast, amino-terminal Pro-containing metallopeptides of either stereochemistry, lacking an extended side chain directed toward the minor groove, did not exhibit a similar diastereoselectivity. While the identity and stereochemistry of amino acids located in the amino-terminal peptide position influenced DNA cleavage, metallopeptide diastereoisomers containing L- and D-Arg (or Lys) within the second peptide position did not exhibit diastereoselective DNA cleavage patterns; simulations indicated that a positively charged amino acid in this location alters the interaction of the metallopeptide equatorial plane and the minor groove leading to an interaction similar to Ni(II)•Gly-Gly-His.

Introduction

Metallopeptides of the general form Ni(II)•Gly-Gly-His contribute to our fundamental understanding of nucleic acid recognition and reactivity through their use in the study of both macromolecule− and small molecule−DNA interactions.[1] These low molecular weight metal−peptide complexes have been applied in the development of synthetic[2] or biosynthetic[3] affinity cleavage, or activity-modulating[4] appendages to DNA binding protein motifs and also occur in the native sequence of DNA associating proteins, such as human protamine P2.[5] Metallopeptides derived from Gly-Gly-His have served also to model Ni-based toxicity and DNA damage events,[5,6] assisted in the development of low molecular weight drug,[7] oligonucleotide,[8] or PNA[9] conjugates, and, as stand-alone metallotripeptides, are agents used to understand fundamental peptide and amino acid interactions with DNA or RNA.[10] Importantly, very recent studies also suggest that Ni(II) and Cu(II)•Gly-Gly-His metallopeptides can serve as models for the development of efficient DNA double strand cleavage agents.[11]

In their earlier role in the study of the Ni(II) and Cu(II) transport domains of the serum albumins, Cu(II)• and Ni(II)•Gly-Gly-His-derived metallopeptides (where Gly can be any α-amino acid) were found to bind metals with high affinity

§ Indiana University—Purdue University Indianapolis.
‡ Howard University.
† Present address: Department of Biochemistry & Molecular Biology, Howard University.

(1) Long, E. C.; Claussen, C. A. In *DNA and RNA Binders: From Small Molecules to Drugs*; Demeunynk, M., Bailly, C., Wilson, W. D., Eds.; Wiley-VCH: New York, 2003; pp 88−125.
(2) (a) Mack, D. P.; Iverson, B. L.; Dervan, P. B. *J. Am. Chem. Soc*. **1988**, *110*, 7572−7574. (b) Mack, D. P.; Dervan, P. B. *J. Am. Chem. Soc*. **1990**, *112*, 4604−4606. (c) Mack, D. P.; Dervan, P. B. *Biochemistry* **1992**, *31*, 9339−9405.
(3) (a) Nagaoka, M.; Hagihara, M.; Kuwahara, J.; Sugiura, Y. *J. Am. Chem. Soc*. **1994**, *116*, 4085−4086. (b) Harford, C.; Narindrasorasak, S.; Sarkar, B. *Biochemistry* **1996**, *35*, 4271−4278.
(4) Mahmoudi, T.; Sarkar, B. *Biopolymers* **1999**, *50*, 273−286.
(5) (a) McKay, D. J.; Renaux, B. S.; Dixon, G. H. *Eur. J. Biochem*. **1986**, *156*, 5−8. (b) Bal, W.; Jezowska-Bojczuk, M.; Kasprazak, K. S. *Chem. Res. Toxicol*. **1997**, *10*, 906−914. (c) Bal, W.; Lukszo, J.; Kasprzak, K. S. *Chem. Res. Toxicol*. **1997**, *10*, 915−921. (d) Bal, W.; Wojcik, J.; Maciejczyk, M.; Grochowski, P.; Kasprzak, K. S. *Chem. Res. Toxicol*. **2000**, *13*, 823−830.
(6) Muller, J. G.; Hickerson, R. P.; Perez, R. J.; Burrows, C. J. *J. Am. Chem. Soc*. **1997**, *119*, 1501−1506.
(7) (a) Grokhovsky, S. L.; Nikolaev, V. A.; Zubarev, V. E.; Surovaya, A. N.; Zhuze, A. L.; Chernov, B. K.; Sidorova, N.; Zasedatelev, A. S. *Mol. Biol. (Moscow)* **1992**, *26*, 1274−1297. (b) Shullenberger, D. F.; Long, E. C. *Bioorg. Med. Chem. Lett*. **1993**, *3*, 333−336. (c) Morier-Teissier, E.; Boitte, N.; Helbecque, N.; Bernier, J. L.; Pommery, N.; Duvalet, J. L.; Fournier, C.; Hecquet, B.; Catteau, J. P.; Henichart, J. P. *J. Med. Chem*. **1993**, *36*, 2084−2090. (d) Steullet, V.; Dixon, D. W. *Bioorg. Med. Chem. Lett*. **1999**, *9*, 2935−2940.
(8) (a) De Napoli, L.; Messere, A.; Montesarchio, D.; Piccialli, G.; Benedetti, E.; Bucci, E.; Rossi, F. *Bioorg. Med. Chem*. **1999**, *7*, 395−400. (b) Truffert, J.-C.; Asseline, U.; Brack, A.; Thuong, N. T. *Tetrahedron* **1996**, *52*, 3005−3016.
(9) Footer, M.; Egholm, M.; Kron, S.; Coull, J. M.; Matsudaira, P. *Biochemistry* **1996**, *35*, 10673−10679.
(10) Long, E. C. *Acc. Chem. Res*. **1999**, *32*, 827−836.
(11) Jin, Y.; Cowan, J. A. *J. Am. Chem. Soc*. **2005**, *127*, 8408−8415.

 10.1021/ja0569757 CCC: $33.50

through the terminal peptide amine, two intervening deprotonated peptide amides, and the His imidazole; these systems exist as well-characterized 1:1 transition metal complexes at physiological pH.[12] Thus, this laboratory has exploited the well-defined structural environment of Ni(II)•Gly-Gly-His-derived metallopeptides toward the understanding of DNA recognition by peptides and amino acids. Given their entirely peptide-based composition, metallopeptides are unique among nucleic acid binding agents in their ability to position along the periphery of a metal complex framework the same chemical functional groups (e.g., guanidinium, amine, and amide moieties) used by proteins and peptide-based natural product antitumor agents for the molecular recognition of DNA and RNA.[13] In addition, the ability to control the orientation of these same side chain functional groups through inversion of the stereochemistry at select α-carbon centers and the potential transformation of peptides into biosynthetic or peptidomimetic agents make Ni(II)•Gly-Gly-His-derived metallopeptides attractive models to increase our knowledge of drug− *and* protein−nucleic acid recognition events.

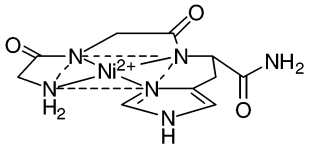

Ni(II)•Gly-Gly-His

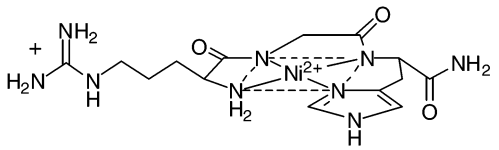

Ni(II)•Arg-Gly-His

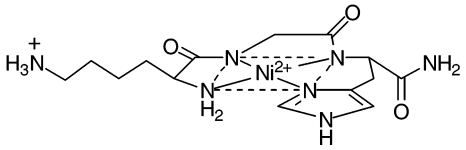

Ni(II)•Lys-Gly-His

We have reported that Ni(II)•Gly-Gly-His-derived metallopeptides cleave DNA site-selectively via C4′−H abstraction as a function of their amino acid composition, stereochemistry, and overall shape. For example, inclusion of Arg or Lys was observed to focus the DNA cleavage of these metallopeptides to the minor groove of A/T-rich regions, while select D-amino acid substitutions produced altered site selectivities.[14,15] More recently, our investigations have focused on defining the minor groove cleavage recognition of these systems through DNA fiber EPR,[16] 1D and 2D NMR, and MD simulations.[17] These studies revealed (1) the stereospecific orientation of M(II)•Arg-Gly-His metallopeptides upon DNA helix association; (2) the insertion of the imidazole and N-terminal "edge" of these approximately square-planar complexes into the minor groove; and (3) potential H-bonding patterns between the imidazole pyrrole N−H, N-terminal N−H protons, and Arg side chain to H-bond acceptors on the floor of the minor groove of an A/T-rich region (i.e., the O2 of T and the N3 of A). Interestingly, these studies suggested a structural similarity between established minor groove binders, such as netropsin, and Ni(II)•Gly-Gly-His metallopeptides along the pathway to DNA cleavage.

The studies described above indicated a structural basis to explain the influence of amino acid stereochemistry in the N-terminal peptide position on the DNA recognition of Ni(II)•Arg-Gly-His: an L-Arg residue aligns along the minor groove to produce an isohelical metallopeptide that facilitates stable small molecule−DNA association, while a D-Arg residue leads to a sterically less complementary metallopeptide diastereomer. Indeed, previous studies have indicated that Ni(II)•Gly-Gly-L-His and Ni(II)•Gly-Gly-D-His display an interesting diastereofacial DNA cleavage selectivity when attached to the DNA binding domain of Hin recombinase,[2b,c] and in our own investigations,[14] we found that substitution of D-His for L-His within Ni(II)•Lys-Gly-His leads to decreased site selectivity. These findings underscored the general importance of diastereoselectivity in the design of DNA-targeted agents and thus prompted us to explore more fully the role of metallopeptide α-carbon stereochemistry on DNA minor groove cleavage recognition. The information gained from such a stereochemical assessment could likely influence the rational design of improved DNA minor groove binding[18] and/or cleavage[11] agents and also reveal structure−activity relationships within some DNA minor groove binding protein motifs.[5] Described herein is a study aimed at understanding the influence of amino acid α-carbon stereochemistry on the DNA minor groove cleavage recognition of Ni(II)•Gly-Gly-His-derived metallopeptides through analyses of site-selective DNA cleavage and molecular simulations based on prior NMR structural investigations.

Results and Discussion

DNA Cleavage Analyses. The site-selective DNA cleavage profiles produced by the diastereomeric metallopeptides Ni(II)•L-Arg-Gly-His and Ni(II)•D-Arg-Gly-His were compared using single-nucleotide resolution polyacrylamide gel analyses (Figure 1 and Supporting Information). The analyses shown in Figure 1 were performed using individually labeled, complementary strands of the same DNA restriction fragment, allowing examination of cleavage patterns present on both antiparallel strands at a given minor groove site. These analyses also included Ni(II)•Gly-Gly-His at a concentration that was 4-fold higher than that of Ni(II)•L/D-Arg-Gly-His to compare the DNA cleavage pattern generated by this "unmodified" metallopeptide to those including alternative side chains. While not specifically examined for the systems investigated herein, prior studies[1,10,14] from our laboratories have demonstrated that Ni(II)•Gly-Gly-His-derived metallopeptides, and diastereomeric pairs thereof, maintain their unique site-selective DNA cleavage profiles as a function of varied metallopeptide concentration; changes in the DNA cleavage site selectivity displayed by a given metal-

(12) (a) Harford, C.; Sarkar, B. *Acc. Chem. Res*. **1997**, *30*, 123−130. (b) Kozlowski, H.; Bal, W.; Dyba, M.; Kowalik-Jankowska, T. *Coord. Chem. Rev*. **1999**, *184*, 319−346.
(13) (a) Steitz, T. A. *Q. Rev. Biophys*. **1990**, *23*, 205−280. (b) Zimmer, C.; Wahnert, U. *Prog. Biophys. Mol. Biol.* **1986**, *47*, 31−112.
(14) Liang, Q.; Eason, P. D.; Long, E. C. *J. Am. Chem. Soc*. **1995**, *117*, 9625−9631.
(15) Liang, Q.; Ananias, D. C.; Long, E. C. *J. Am. Chem. Soc*. **1998**, *120*, 248−257.
(16) Nagane, R.; Koshigoe, T.; Chikira, M.; Long, E. C. *J. Inorg. Biochem*. **2001**, *83*, 17−23.
(17) Fang, Y.-Y.; Ray, B. D.; Claussen, C. A.; Lipkowitz, K. B.; Long, E. C. *J. Am. Chem. Soc*. **2004**, *126*, 5403−5412.
(18) Renneberg, D.; Dervan, P. B. *J. Am. Chem. Soc*. **2003**, *125*, 5707−5716.

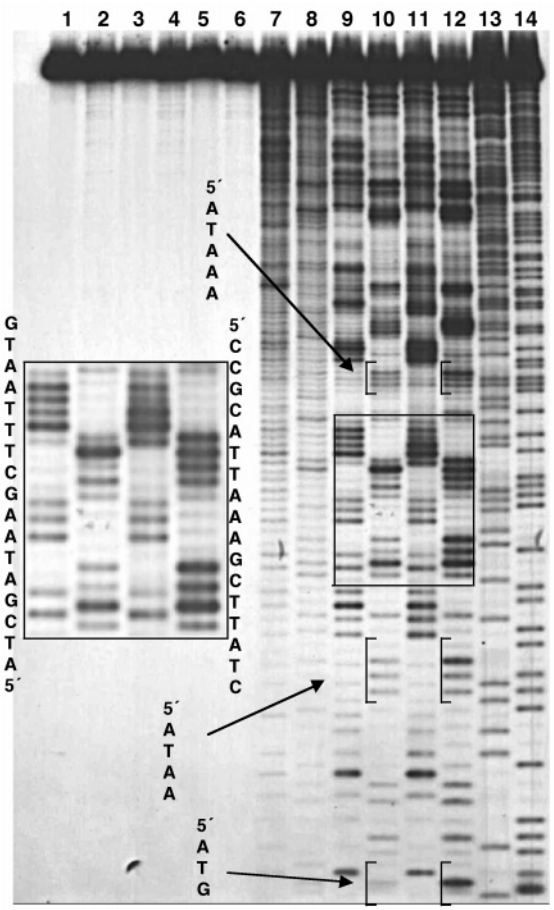

Figure 1. Autoradiogram of Ni(II)•L/D-Arg-Gly-His and Ni(II)•Gly-Gly-His induced cleavage of a 5′- and 3′-^{32}P-end labeled 167 base pair DNA restriction fragment from pBR322 (Eco RI → Rsa I). Each lane contained 50 μM DNA (base pair concentration) and 25 μM cleavage agent + 25 μM $KHSO_5$ in 10 mM Na−cacodylate buffer, pH 7.5; Ni(II)•Gly-Gly-His cleavage reactions were carried out at 4-fold higher concentrations. Reaction times were 1 min at room temperature. Odd numbered lanes contained 5′-end labeled DNA, while even numbered lanes contained 3′-end labeled DNA fragments. Lanes 1 and 2, intact DNA + 100 μM $KHSO_5$. Lanes 3 and 4, reaction controls (100 μM $Ni(OAc)_2$ + 100 μM $KHSO_5$). Lanes 5 and 6, reaction controls (100 μM Gly-Gly-His + 100 μM $KHSO_5$). Lanes 7 and 8, 100 μM Ni(II)•Gly-Gly-His + 100 μM $KHSO_5$. Lanes 9 and 10, 25 μM Ni(II)•L-Arg-Gly-His. Lanes 11 and 12, 25 μM Ni(II)•D-Arg-Gly-His. Lanes 13 and 14, Maxam−Gilbert A+G sequencing reactions.

lopeptide are not observed as a function of concentration other than uniform increases or decreases in overall cleavage intensity.

As illustrated in Figure 1 (and Supporting Information), the DNA cleavage patterns induced by both Arg-containing metallopeptide diastereoisomers (lanes 9/10 and 11/12) were more intense and clearly focused on A/T-rich regions in comparison to Ni(II)•Gly-Gly-His (lanes 7/8); however, distinct differences between the site selectivities and relative cleavage intensities of targeted nucleotides within particular sites can be readily observed at identical concentrations of the Arg diastereomeric metallopeptides. In comparison, Ni(II)•Gly-Gly-His produced a relatively low level of DNA cleavage intensity that, while generally random with respect to its site selectivity, was somewhat reminiscent of Ni(II)•L-Arg-Gly-His. A comparison of Ni(II)•L-Arg-Gly-His with Ni(II)•D-Arg-Gly-His revealed that cleavage by the L-isomer (lanes 9/10) occurred more selectively than for the D-isomer (lanes 11/12) at most A/T-rich sites. As emphasized in the region expanded in the inset within Figure 1, there are differences in the patterns and ratios of cleavage selectivity between these two metallopeptide diastereoisomers, in particular, at the 5′-ATTAAA and the 5′-TTATC sites contained within the 3′-end labeled fragments (even numbered lanes) and the complementary 5′-TTTAAT site contained within the 5′-end labeled fragments (odd numbered lanes). In these cases, the cleavage patterns produced by Ni(II)•D-Arg-Gly-His become less focused within a given sequence, resulting in multiple adjacent cleaved nucleotides, while Ni(II)•L-Arg-Gly-His generally produced only one or two strong primary cleavage bands at a particular A/T-rich site. In addition to the region expanded in Figure 1, three independent 5′-AT-Pu sites (within 5′-ATAAA, 5′-ATAA, and 5′-ATG) found within the 3′-end labeled fragment (shown with brackets in Figure 1) indicated consistent increased cleavage by the D-Arg diastereoisomer at the T residue of 5′-AT-Pu, while the L-Arg diastereomer either did not lead to cleavage or resulted in only weak cleavage throughout the site.

Along with our comparison of Ni(II)•L-Arg-Gly-His and Ni(II)•D-Arg-Gly-His, we also examined the general nature of the above observations using a different DNA restriction fragment and Ni(II)•L-Lys-Gly-His and Ni(II)•D-Lys-Gly-His in direct comparison to Ni(II)•L-Arg-Gly-His and Ni(II)•D-Arg-Gly-His (Supporting Information). The overall patterns of site-selective DNA cleavage produced by the Arg- and Lys-containing diastereomeric metallopeptides in these experiments were virtually identical. Specifically, the metallopeptides that contain D-Arg or D-Lys in the amino-terminal peptide position consistently resulted in less selectivity within a given cleaved region of the DNA substrate, while inclusion of either an L-Arg or L-Lys produced a relative increase in DNA site selectivity. These observations verified that Arg and Lys are functionally equivalent within a given metallopeptide,[14−17] leading to similar minor groove-associated structures as supported also by NMR investigations.[17] This analysis also included Ni(II)•Gly-Gly-His and Ni(II)•L/D-Ala-Gly-His as additional controls (Supporting Information); at concentrations equivalent to the Arg and Lys metallopeptides, DNA cleavage was not detected for these charge-neutral metallopeptides. These data demonstrate that the DNA cleavage recognition process catalyzed by Ni(II)•Gly-Gly-His metallopeptides is diastereoselective when an amino acid residue with an extended side chain, such as Arg or Lys, is present in the amino-terminal peptide position; while the same locations are targeted by each member of a diastereoisomeric pair, metallopeptide structural variations appear to promote significant differences in the details of their final cleavage selectivity within a given A/T-rich site.

Along with our examination of the diastereoselective DNA cleavage exhibited by the Ni(II)•L/D-Arg-Gly-His and Ni(II)•L/D-Lys-Gly-His pairs, we also examined the site-selective DNA cleavage induced by Ni(II)•L/D-Pro-Gly-His metallopeptides. Previously, Ni(II)•L-Pro-Gly-His, despite being a charge-neutral metallopeptide, was found to increase DNA cleavage to a level comparable to that found with Lys- or Arg-substituted metallopeptides.[19] For the purposes of the present study, Ni(II)•L/D-Pro-Gly-His thus provided a cleavage-active metallopeptide system that differs substantially from Arg- or Lys-containing metallopeptides with extended, flexible side chains in that the Pro side chain is compact and rigidly constrained.

(19) Huang, X.; Pieczko, M. E.; Long, E. C. *Biochemistry* **1999**, *38*, 2160−2166.

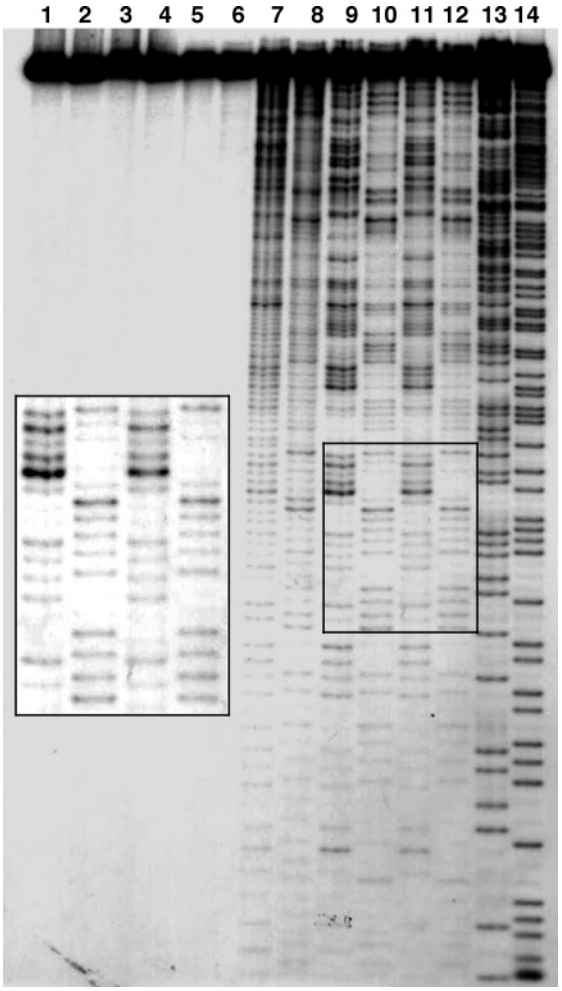

Figure 2. Autoradiogram of Ni(II)•L/D-Pro-Gly-His and Ni(II)•Gly-Gly-His induced cleavage of a 5′- and 3′-^{32}P-end labeled 167 base pair DNA restriction fragment from pBR322 (Eco RI → Rsa I). Each lane contained 50 μM DNA (base pair concentration) and 25 μM cleavage agent + 25 μM $KHSO_5$ in 10 mM Na−cacodylate buffer, pH 7.5; Ni(II)•Gly-Gly-His cleavage reactions were carried out at 4-fold higher concentrations. Reaction times were 1 min at room temperature. Odd numbered lanes contained 5′-end labeled DNA, while even numbered lanes contained 3′-end labeled DNA fragments. Lanes 1 and 2, intact DNA + 100 μM $KHSO_5$. Lanes 3 and 4, reaction control (100 μM $Ni(OAc)_2$ + 100 μM $KHSO_5$). Lanes 5 and 6, reaction control (100 μM Gly-Gly-His + 100 μM $KHSO_5$). Lanes 7 and 8, 100 μM Ni(II)•Gly-Gly-His + 100 μM $KHSO_5$. Lanes 9 and 10, 25 μM Ni(II)•L-Pro-Gly-His. Lanes 11 and 12, 25 μM Ni(II)•D-Pro-Gly-His. Lanes 13 and 14, Maxam−Gilbert A+G sequencing reactions. See Figure 1 for the sequence of the inset region shown.

As shown in Figure 2, analysis of the Ni(II)•L-Pro-Gly-His- and Ni(II)•D-Pro-Gly-His-mediated cleavage of DNA restriction fragments (5′- and 3′-end labeled from the same source as those employed in the analysis shown in Figure 1) revealed patterns of site-selective DNA modification that differed from those produced by Ni(II)•L/D-Arg-Gly-His. While low-intensity cleavage can be seen within DNA sites that are targeted also by Ni(II)•Arg-Gly-His, cleavage within the region highlighted in Figure 2 by the Ni(II)•L/D-Pro-Gly-His metallopeptides was almost exclusively limited to the 5′-TTTAAT site and its complementary sequence 5′-ATTAAA. Key differences between the overall site selectivities of Ni(II)•Arg-Gly-His and Ni(II)•Pro-Gly-His are expected given their differences in amino acid composition. However, more important, a comparison of the activities of the Ni(II)•Pro-Gly-His diastereoisomers revealed that they, unlike the distinctions found between the Ni(II)•Arg-Gly-His diastereoisomers, produced almost identical patterns of DNA modification for both the 5′- and 3′-end labeled DNA restriction fragments employed in this analysis.

The results presented above indicate that a rigid, compact amino acid side chain, such as Pro, in the amino-terminal peptide position is incapable of eliciting a diastereoselective DNA interaction within the metallopeptide framework, in contrast to a relatively large, flexible Arg or Lys side chain. Given the demonstrated impact of amino acid stereochemistry within the amino-terminal peptide position, we sought to examine the effect also in the second peptide position of the metallopeptide framework. Accordingly, DNA cleavage by Ni(II)•Gly-L/D-Arg-His and Ni(II)•Gly-L/D-Lys-His was also examined.

The site-selective DNA cleavage patterns generated by Ni(II)•Gly-L/D-Arg-His, Ni(II)•Gly-L/D-Lys-His, and Ni(II)•Gly-Gly-His were compared using 3′-end labeled DNA restriction fragments, as shown in Figure 3. These gel analyses indicate that the Ni(II)•Gly-L/D-Arg-His and Ni(II)•Gly-L/D-Lys-His metallopeptide isomers did not exhibit the diastereoselectivity observed with the amino-terminal Arg- or Lys-substituted metallopeptides; DNA cleavage by all metallopeptides examined in this particular gel resulted in virtually identical cleavage patterns. As in previous analyses, Ni(II)•Gly-Gly-His was examined in parallel at an increased metallopeptide:DNA ratio to facilitate a comparison of the activity of substituted versus nonsubstituted complexes. The site selectivity of Ni(II)•Gly-Gly-His-induced DNA cleavage observed was largely indistinguishable from the Arg or Lys second-position-substituted metallopeptides. While these data revealed that Arg/Lys substitutions within the second peptide position do not exhibit the diastereoselectivity observed upon amino-terminal position substitution, it is also interesting to note that (1) an overall increase in metallopeptide concentration was necessary to produce a cleavage intensity comparable to that of the corresponding amino-terminal-substituted metallopeptides; and (2) the cleavage efficiencies displayed by the D-amino acid metallopeptides, Ni(II)•Gly-D-Arg-His and Ni(II)•Gly-D-Lys-His, were consistently greater than those of the corresponding L-amino acid metallopeptides. These observations further support the notion that the second peptide position influences metallopeptide−DNA recognition differently and less than does the amino-terminal position.

The DNA cleavage analyses described above are in accord with our experimental understanding of metallopeptide−DNA recognition reported previously. With the amino-terminal amine and His imidazole edge of a particular metallopeptide inserted into the minor groove of DNA, the amino-terminal amino acid side chain is also inserted into the minor groove and can influence the DNA interaction of the metallopeptide equatorial plane; this effect appears to be accentuated by the presence of extended amino acid side chains, such as Arg or Lys, but not by a side chain substitution, such as Pro. In comparison, the amino acid side chain located at the second peptide position projects outward from the DNA helical axis and is perhaps less able to influence the cleavage-productive "approach" or final positioning of the metallopeptide to a given DNA recognition site. As outlined below, these hypotheses were tested further through the use of molecular modeling and molecular dynamics simulations.

Molecular Modeling and Simulations: General Considerations. Computational studies of Ni(II)•Gly-Gly-His-derived

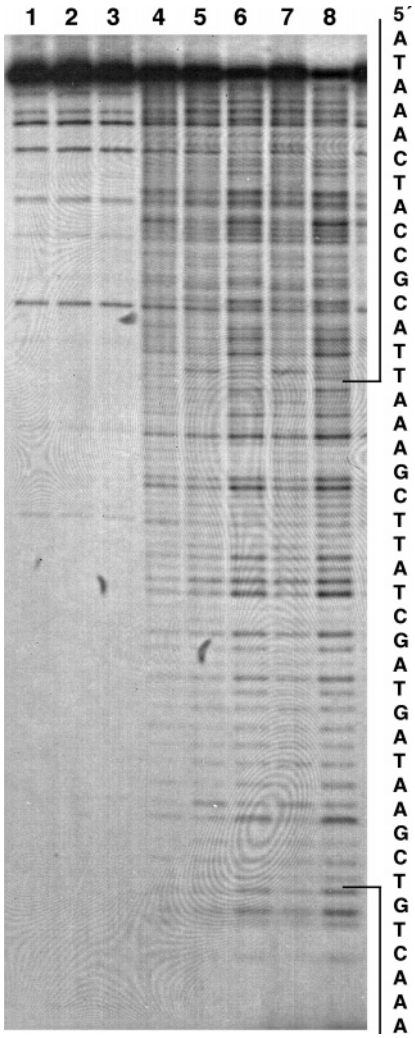

Figure 3. Autoradiogram of Ni(II)•Gly-L/D-Arg-His, Ni(II)•Gly-L/D-Lys-His, and Ni(II)•Gly-Gly-His induced cleavage of a 3′-^{32}P-end labeled 167 base pair DNA restriction fragment from pBR322 (Eco RI → Rsa I). Each lane contained 50 μM DNA (base pair concentration) and 50 μM cleavage agent + 50 μM $KHSO_5$ in 10 mM Na−cacodylate buffer, pH 7.5; Ni(II)•Gly-Gly-His cleavage reactions were carried out at 4-fold higher concentrations. Reaction times were 1 min at room temperature. Lane 1, intact DNA. Lane 2, reaction control (100 μM $Ni(OAc)_2$ + 100 μM $KHSO_5$). Lane 3, reaction control (200 μM Gly-Gly-His + 200 μM $KHSO_5$). Lane 4, 200 μM Ni(II)•Gly-Gly-His + 200 μM $KHSO_5$. Lanes 5 and 6, 50 μM Ni(II)•Gly-L/D-Arg-His, respectively. Lanes 7 and 8, 50 μM Ni(II)•Gly-L/D-Lys-His, respectively.

metallopeptides bound to the A/T-rich minor groove of d(CGCGAATTCGCG)$_2$ were carried out as described previously[17] through molecular modeling and simulation protocols similar to those employed by Wellenzohn and co-workers.[20−22] As used successfully in prior studies, the starting point for these investigations involved the crystal structure[23] of netropsin-bound d(CGCGAATTCGCG)$_2$ [or d(CGCGTTAACGCG)$_2$[24] used in addition with the Pro-containing systems] that generated minor groove binding sites by replacing netropsin with a Ni(II)•Gly-Gly-His-derived metallopeptide.[17,25] Eight 1500 ps molecular dynamics simulations were carried out in an explicit solvent bath of water for DNA + Ni(II)•Gly-Gly-His, DNA + Ni(II)•Gly-L/D-Arg-His, DNA + Ni(II)•L-Lys-Gly-His, and DNA (AATT and TTAA oligonucleotides) + Ni(II)•L/D-Pro-Gly-His (see Supporting Information).

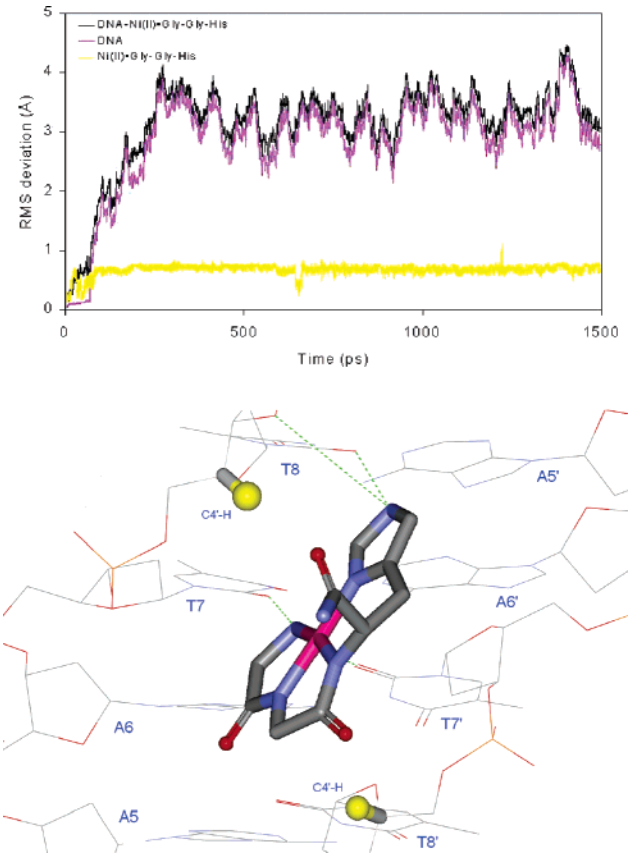

Figure 4. RMS deviations with respect to the starting structure in the simulation of Ni(II)•Gly-Gly-His bound to d(CGCGAATTCGCG)$_2$ (upper panel) and average structure representation of the H-bonds observed upon simulation of Ni(II)•Gly-Gly-His bound to d(CGCGAATTCGCG)$_2$ (lower panel); the H-bonds formed between the His imidazole N−H and the O2 of T8 occur only transiently.

Simulation of Ni(II)•Gly-Gly-His and Comparison to Ni(II)•L/D-Arg-Gly-His. Root mean square (RMS) deviations were used to assess the relative motion of each DNA-bound metallopeptide. As shown in Figure 4, the RMS deviations of Ni(II)•Gly-Gly-His + DNA and the DNA alone are similar but deviate consistently from each other (ca. 0.04 Å) with the average RMS value of the ligand being 0.69 Å. These results indicate that the flexibility of the DNA backbone contributed to most of the RMS changes, while at the same time, the metallopeptide remained rigid and moved independent of the minor groove, as expected from the weak DNA binding of this particular charge-neutral metallopeptide.[17]

Further analysis of the simulation supports the initial observations noted above (Supporting Information). The interaction of Ni(II)•Gly-Gly-His and the minor groove was observed to occur mainly through the amino-terminal N−H protons to the O2 of T7 on complementary DNA strands. This interaction holds Ni(II)•Gly-Gly-His loosely in the minor groove at the center of

(20) Wellenzohn, B.; Winger, R. H.; Hallbrucker, A.; Mayer, E.; Liedl, K. R. *J. Am. Chem. Soc.* **2000**, *122*, 3927−3931.
(21) Wellenzohn, B.; Flader, W.; Winger, R. H.; Hallbrucker, A.; Mayer, E.; Liedl, K. R. *Biophys. J.* **2001**, *81*, 1588−1599.
(22) Flader, W.; Wellenzohn, B.; Winger, R. H.; Hallbrucker, A.; Mayer, E.; Liedl, K. R. *J. Phys. Chem. B.* **2001**, *105*, 10379−10387.
(23) Sriram, M.; van der Marel, G. A.; Roelen, H. L.; van Boom, J. H.; Wang, A. H. J. *Biochemistry* **1992**, *31*, 11823−11834.
(24) Balendiran, K.; Rao, S. T.; Sekharudu, C. Y.; Zon, G.; Sundaralingam, M. *Acta Crystallogr. D* **1995**, *51*, 190−198.
(25) Bal, W.; Djuran, M. I.; Margerum, D. W.; Gray, E. T.; Mazid, M. A.; Tom, R. T.; Nieboer, E.; Sadler, P. J. *J. Chem. Soc., Chem. Commun.* **1994**, 1889−1890.

the A/T-rich region, allowing a clockwise and counterclockwise rotation of the His imidazole in and out of the minor groove. Without additional stable H-bonds from the His imidazole pyrrole N−H and a side chain located in the first peptide position, as found with Ni(II)•Arg-Gly-His,[17] the amino-terminal N−H interaction of Ni(II)•Gly-Gly-His alone cannot hold this ligand as rigidly and firmly in the minor groove as observed with Ni(II)•L-Arg-Gly-His. In addition, as observed in the average structure of the DNA + Ni(II)•Gly-Gly-His (Supporting Information), these interactions, in total, impose very little change on the backbone structure of the DNA. Thus, Ni(II)•Gly-Gly-His is unable to form a complementary set of H-bonds, preventing a well-defined cleavage recognition of the minor groove, as observed experimentally.

In contrast to Ni(II)•Gly-Gly-His, the Ni(II)•L/D-Arg-Gly-His diastereomers interact with features of the central A/T-rich minor groove using three H-bond donors: (1) the imidazole pyrrole N−H; (2) the amino-terminal N−H protons; and (3) the Arg side chain guanidinium moiety.[17] While both diastereomeric metallopeptides were found to be capable of employing all three of these donors in the minor groove interaction, there are fundamental differences between how each diastereomer uses these functionalities to make contact with the DNA, likely accounting for the distinct differences in their observed DNA cleavage recognition properties.

In the simulation of DNA + Ni(II)•L-Arg-Gly-His, the RMS deviations indicated that, in comparison to Ni(II)•Gly-Gly-His, this metallopeptide diastereomer fits snuggly in the minor groove with little independent motion.[17] The metallopeptide and the DNA maintained an overall complementarity; that is, as the DNA moved, the metallopeptide flexed along with it. Indeed, both visual and numerical analyses of the simulation trajectory demonstrated that the metallopeptide did not reposition upon equilibration, but instead maintained the positioning of the metal complex coordination plane parallel to, and equidistant from, both walls of the minor groove. This positioning and tight complementary fit is due to the ability of Ni(II)•L-Arg-Gly-His to form H-bond contacts with the floor of the minor groove via (1) the His imidazole pyrrole N−H; (2) the amino-terminal N−H protons; and (3) the Arg side chain that was positioned, like the guanidinium moiety of netropsin, between the walls of the minor groove to make contact with the floor of the minor groove. The former two contacts served to anchor the equatorial plane of the metallopeptide in the minor groove, while that of the side chain (as aided by its α-carbon stereochemistry) generated a third point of interaction that supported this positioning and its stability; that is, the side chain functioned as a stabilizing "outrigger". Overall, the Ni(II)•L-Arg-Gly-His diastereoisomer adopted a DNA-bound isohelical fit that complemented well the curvature, width, and H-bonding capabilities of the A/T-rich DNA minor groove, forming a stable interaction that did not reposition once bound (Figure 5). These observations are entirely consistent with the cleavage results presented earlier and explain the focused cleavage seen within a given A/T-rich site.

Unlike the L-Arg isomer, Ni(II)•D-Arg-Gly-His, while interacting with the A/T-rich minor groove using a similar set of metallopeptide donors, was found to be less stable, acted independent of the DNA, and shifted position within the A/T-rich region during the simulation as evidenced by both the RMS deviations and trajectory analysis.[17] With Ni(II)•D-Arg-Gly-His, the D-Arg stereochemistry created a steric block causing the metallopeptide to form only partial contacts with the floor of the minor groove, especially the crucial contacts that form with the amino-terminal N−H protons. Thus, lacking the complementary isohelical fit of the L-Arg stereoisomer (Figure 5), Ni(II)•D-Arg-Gly-His maintains its structural independence and alternates between two sets of contact points on opposite sides of the minor groove. Ni(II)•D-Arg-Gly-His also slides along the A/T-rich minor groove floor, putting it in proximity to multiple target nucleotides and their respective C4′−H positions; however, the "weakened" interaction of Ni(II)•D-Arg-Gly-His is not simply like that of Ni(II)•Gly-Gly-His because three potential points of contact still drive targeting to A/T-rich regions.

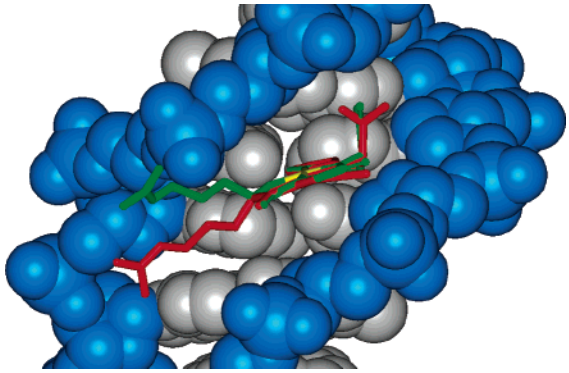

Figure 5. Overlay of space-filling models emphasizing the differences in the locations of the side chains of Ni(II)•L-Arg-Gly-His (red) in comparison to Ni(II)•D-Arg-Gly-His (green) while bound to $d(CGCGAATTCGCG)_2$. While these static models do not adequately portray the dynamics of these systems, they do serve to illustrate the gross differences observed.

The above results illustrate the general functional importance of a positively charged amino acid side chain outrigger and the influence of its stereochemically determined positioning on DNA minor groove−small molecule targeting; however, as shown in our experimental analyses, the exact chemical nature of the side chain (i.e., a guanidinium vs an ϵ-amine) appears to be less important than its stereochemistry. As noted earlier, the Ni(II)•L/D-Lys-Gly-His diastereoisomers were able to cleave DNA in a fashion identical to their respective Ni(II)•Arg-Gly-His isomers, albeit with less efficiency.[26] Accordingly, we examined the behavior of the Ni(II)•L-Lys-Gly-His diastereomer, an alternative example of a metallopeptide with a functional, positively charged side chain.

Simulation of Ni(II)•L-Lys-Gly-His−An Alternative Outrigger. As shown in Figure 6, the RMS deviations of the simulations of Ni(II)•L-Lys-Gly-His + DNA, DNA alone, and Ni(II)•L-Lys-Gly-His alone exhibit a close similarity to those of DNA + Ni(II)•L-Arg-Gly-His. The RMS deviations of Ni(II)•L-Lys-Gly-His and DNA alone coincide during the simulation; the average RMS value found for DNA + Ni(II)•L-Lys-Gly-His was 3.94 Å, in comparison to 3.39 Å, the average RMS value found for DNA + Ni(II)•L-Arg-Gly-His. These comparable values indicate that Ni(II)•L-Lys-Gly-His, upon association with the A/T-rich minor groove, moves and flexes with the DNA backbone in a complementary fashion, as similarly described for Ni(II)•L-Arg-Gly-His. Indeed, further analysis of the simulation confirmed that Ni(II)•L-Lys-Gly-His behaved very much

(26) Liang, Q. Ph.D. Dissertation, Purdue University, Indianapolis, IN, 1997.

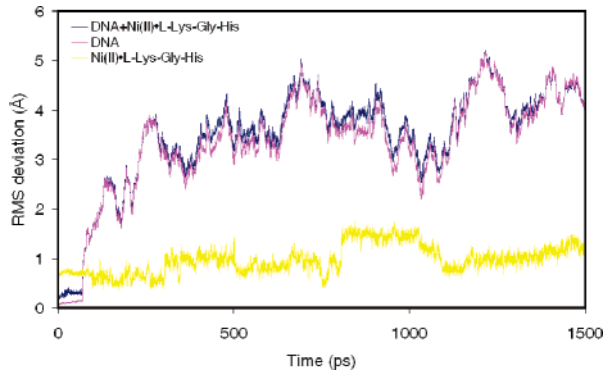

Figure 6. RMS deviations with respect to the starting structure in the simulation of Ni(II)•L-Lys-Gly-His bound to d(CGCGAATTCGCG)$_2$.

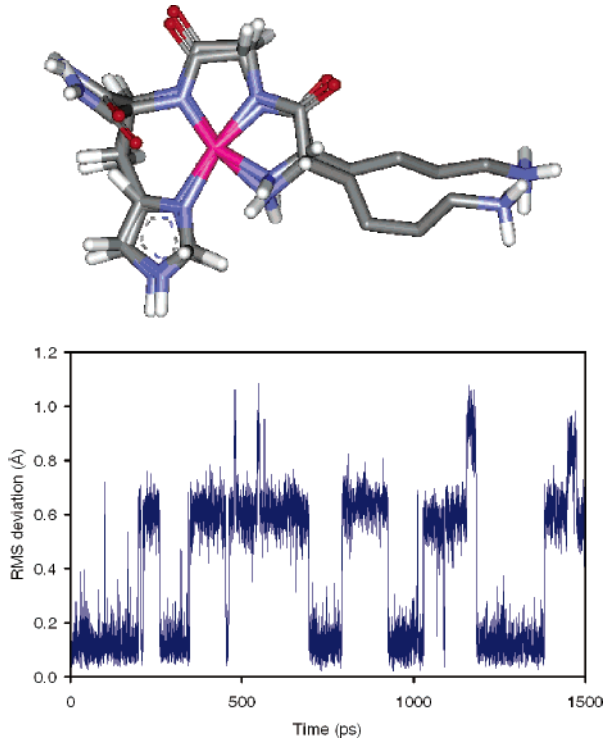

Figure 7. Comparison of the two resulting metallopeptide structures with different side chain conformations observed during the simulation of Ni(II)•L-Lys-Gly-His bound to the minor groove of d(CGCGAATTCGCG)$_2$ (upper panel), and the RMS deviation of the side chain of Ni(II)•L-Lys-Gly-His with respect to the starting structure revealing the conformation shifting that occurs (lower panel).

like Ni(II)•L-Arg-Gly-His (Supporting Information). The key difference observed in comparing the simulations of minor groove-bound Ni(II)•L-Lys-Gly-His and Ni(II)•L-Arg-Gly-His is that the side chain of Lys alternates between two conformations as it interacts with the DNA minor groove (Figure 7). As a consequence, the ϵ-amino outrigger of Ni(II)•L-Lys-Gly-His is unable to interact with the minor groove as strongly as can the guanidinium-functionalized outrigger of Ni(II)•L-Arg-Gly-His.

Our simulations of Ni(II)•L-Lys-Gly-His and DNA thus indicate an interaction that is almost identical to that of Ni(II)•L-Arg-Gly-His but understandably weaker, as observed early on in studies of supercoiled cccDNA cleavage,[26] because the influential outrigger of the metallopeptide, in the form of an L-Lys side chain, associates with the minor groove neither as tightly nor with the stability of a guanidinium-containing L-Arg. These observations are consistent with, and explain, the results of the DNA cleavage gels presented herein, and elsewhere,[26] and also suggest a chemical rationale for the predominance of guanidinium-containing functionalities in DNA-targeted natural products in contrast to the evolution of compounds with simple amine functionalities.

Simulations of Ni(II)•L-Pro-Gly-His and Ni(II)•D-Pro-Gly-His. As demonstrated via restriction fragment cleavage, metallopeptides containing an amino-terminal Pro residue do not display a distinct diastereoselectivity. To explore the possible basis for this difference, the Ni(II)•L/D-Pro-Gly-His systems were examined. In the case of these particular simulations, not only employed was the AATT substrate but also a substrate containing a TTAA site[24] given the cleavage recognition noted earlier.

As with the other systems, RMS deviations were used to assess the simulations (Supporting Information). Subsequently, examination of the trajectories revealed that during the AATT simulations both Pro-containing metallopeptide diastereomers shifted one base pair from the center of GAATTC, a relatively narrow (10.4 Å) location in the unbound DNA, to the center of GAAT, which constitutes a slightly wider (11.4 Å) region of the minor groove (Supporting Information).[21] Indeed, with the TTAA substrate, in comparison, the slightly wider groove width present at the TTAA site (12.6 Å) permitted a more stable interaction, as evidenced by a lack of metallopeptide shifting along the minor groove. In comparison to the Arg- and Lys-containing metallopeptides, the Pro-containing metallopeptides are larger, consequently requiring accommodation in a slightly wider portion of the minor groove. In both cases also, the pyrrole N−H of the His imidazole plays the primary role in forming interactions between the Pro metallopeptides and the minor groove floor; blocked by the constrained five-membered ring of Pro, the N−H proton of the terminal Pro imine cannot interact with H-bond acceptors on the floor of the minor groove (Figure 8). With TTAA, the pyrrole N−H of both diastereomers interacts with acceptors on complementary DNA strands of this symmetrical site (Figure 8) while maintaining a similar overall groove interaction, as reflected in their identical cleavage activities. To some extent, the Pro metallopeptides represent the opposite case scenario in comparison to Ni(II)•Gly-Gly-His that uses the amino-terminal amine almost exclusively.

As before, the results of our experimental studies and simulations coincide: (1) the DNA cleavage patterns of the two Pro isomers are virtually identical as are their simulations; and (2) we also observe that TTAA sites appear to promote a more stable interaction and constitute preferred, experimentally determined cleavage sites. Thus, these two metallopeptide diastereomers interact similarly with the DNA minor groove, supporting the notion that an extended appendage directed into the minor groove can influence binding/cleavage behavior to a far greater extent than a compact, rigid structure.

Simulation of Ni(II)•Gly-L/D-Arg-His: Repositioning the Outrigger. Having examined the influence of a positively charged side chain when located in the first peptide position, we also examined the influence of such an appendage when contained within the second peptide position in an attempt to explain the DNA cleavage data obtained for Ni(II)•Gly-L/D-Arg-His. As shown in Figure 9, the RMS changes of the metallopeptide + DNA complexes and the DNA alone are

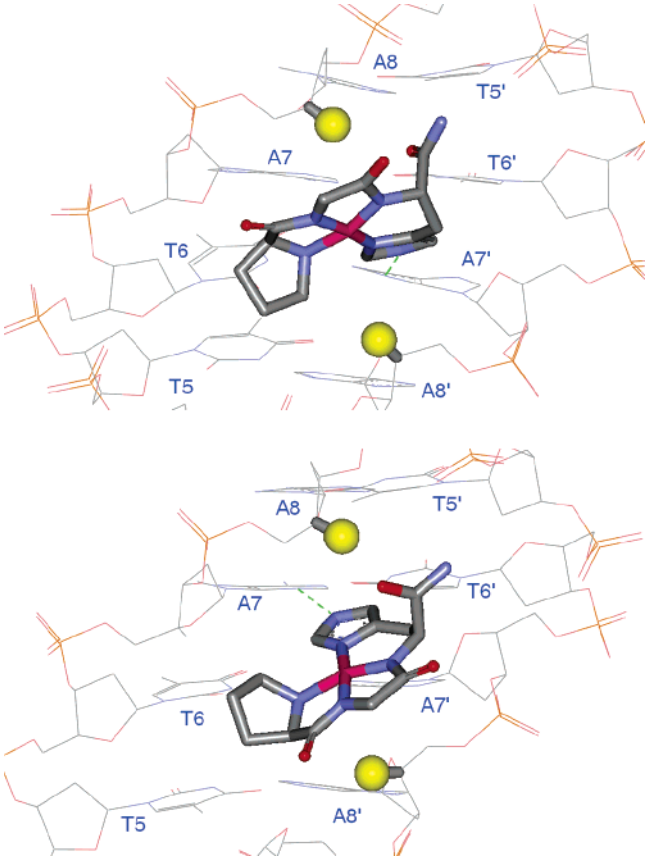

Figure 8. Average structure representations of the H-bonds observed upon simulation of Ni(II)•L-Pro-Gly-His (top) and Ni(II)•D-Pro-Gly-His (bottom) bound to the minor groove of d(CGCGTTAACGCG)$_2$; yellow atoms highlight the proximity of C4′−H positions.

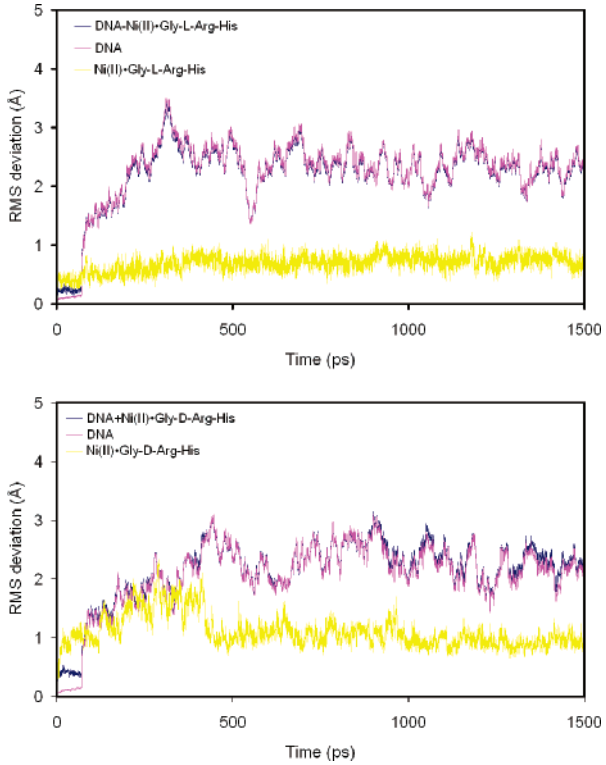

Figure 9. RMS deviations of the simulation of Ni(II)•Gly-L-Arg-His (top) and Ni(II)•Gly-D-Arg-His (bottom) bound to d(CGCGAATTCGCG)$_2$ with respect to the starting structures of the complex, the DNA alone, and ligand alone.

nearly identical and coincide in simulations of both isomeric systems when bound to d(CGCGAATTCGCG)$_2$. These data indicate that the ligands behave similarly and do not move within the minor groove or change their structures substantially in comparison to Ni(II)•L-Arg-Gly-His. For comparison, the average RMS values of the DNA + Ni(II)•Gly-L-Arg-His and DNA + Ni(II)•Gly-D-Arg-His systems are 2.33 and 2.32 Å, respectively, lower than the value of 3.39 Å calculated for Ni(II)•L-Arg-Gly-His (Supporting Information).

Along with the assessment of RMS deviations, the trajectory shows that both Ni(II)•Gly-L-Arg-His and Ni(II)•Gly-D-Arg-His remain parallel to the walls of the minor groove at the center of the A/T-rich region (Supporting Information). During the course of both simulations, the pyrrole N−H of the His imidazole rotates away from the minor groove floor and points to the edge of the minor groove. Analysis of the H-bonds formed show that both Ni(II)•Gly-L-Arg-His and Ni(II)•Gly-D-Arg-His bind to the minor groove of DNA like Ni(II)•Gly-Gly-His, mainly through the amino-terminal N−H protons to O2 of T7 on two strands. Meanwhile, the guanidinium "tail" of both metallopeptides bends toward the minor groove and interacts with acceptors along its edge. With this particular positioning of the Arg side chain in the second peptide position, differences in α-carbon stereochemistry do not appear to influence the final interaction overtly, thus leading to very similar minor groove-bound structures for both diastereomeric metallopeptides; it appears that a strong attraction between the minor groove and the positively charged side chain in its position outside the minor groove serves to disrupt the imidazole−minor groove interaction. These observations suggest a plausible rationale for why these two diastereomeric metallopeptides exhibit a site selectivity that is similar to one another and both closely resembling that produced by Ni(II)•Gly-Gly-His, which also rotates its imidazole functionality out of the minor groove.

While the Ni(II)•Gly-L/D-Arg-His systems interact with the DNA minor groove in a fashion resembling one another and that of Ni(II)•Gly-Gly-His, the diastereomers do, however, differ with regards to the overall "thickness" of the equatorial planes of each system. A comparison of the shape and minor groove fit of these diastereomeric metallopeptides (Supporting Information) indicates that the D-Arg/Lys systems are less sterically hindered due to the in-plane positioning of the Xaa$_2$ side chain. This allows an easier overall approach and deeper insertion into the minor groove; the L-Arg/Lys systems, while able to interact similarly with the minor groove, are somewhat more sterically hindered, impeding their approach to the minor groove, resulting in a decrease in overall cleavage efficiency, as observed experimentally. We have noted a quite similar observation in our earlier analysis of L-His versus D-His diastereomeric metallopeptides[14] due, in this case, to the stereochemical placement of the carboxy-terminal amide functionality. Again, analysis of the MD simulation has served to assist in understanding the experimentally determined behavior of these systems.

Summary and Conclusions

The work described herein couples experimental observations of DNA cleavage site selectivity with molecular dynamics simulations to reveal and rationalize characteristics of various

Table 1. Summary of Ni(II)•Xaa_1-Xaa_2-His_3 Activities as a Function of Xaa Position and Configuration

	DNA cleavage recognition characteristics
	Xaa_1
Gly	low efficiency DNA cleavage, slight preference for A/T-rich regions
Arg/Lys	strong, A/T-selective DNA cleavage focused to a subset of available A/T nucleotides when in the L-configuration; less focused A/T-selective cleavage when in the D-configuration
Pro	A/T-selective DNA cleavage focused to a subset of available nucleotides; selectivity for TTAA sites; no observed differences between the activities of L-Pro and D-Pro
Ala/Asn[a]	Gly-like DNA cleavage efficiency and selectivity
	Xaa_2
Gly	low efficiency DNA cleavage; slight preference for A/T-rich regions
Arg/Lys	Gly-like site selectivity when in L- or D-configuration but with slightly increased cleavage efficiency; cleavage efficiency of D-Xaa > L-Xaa
Asn[a]	Gly-like DNA cleavage site selectivity when in L-configuration; alternative 5′-CCT site selectivity when in D-configuration, modeling suggests steric hindrance on one "face" of the complex introduced by the D-Asn side chain amide
	His_3[a]
	increased site selectivity when L; decreased when D; modeling suggests that the steric hindrance of the C-terminal amide in L-His is > D-His; D-His metallopeptides are narrower and fit more easily into the minor groove.

[a] From refs 1, 10, 14, and 26.

Ni(II)•Gly-Gly-His-derived metallopeptide−minor groove interactions. We find that metallopeptides with extended Arg or Lys side chains directed into the minor groove produce a diastereoselective DNA cleavage interaction, while nonextended side chains, as found in Pro residues, do not bring about a similar diastereoselective response. In addition, positively charged Arg and Lys substitutions at locations not directed toward any distinct structural feature of the DNA target, as in the second peptide position of Ni(II)•Gly-Gly-His, do not exhibit a similar diastereoselectivity but can nonetheless influence cleavage site selectivity and cleavage efficiency through the alteration of other, usually stabilizing, interactions. Observations from the work described herein, accompanied by our earlier published observations[1,10,14,26] describing the activity of select metallopeptide diastereomers are summarized in Table 1.

It is noteworthy that while the DNA cleavage reactivities exhibited by the metallopeptides described herein are predominantly focused to nonhomopolymeric A/T-rich DNA regions, we do not rule out the possibility of metallopeptide interaction *unaccompanied* by reactivity at canonical G/C sites. To date, all experimental results suggest that minor groove width and accessibility, and not simply nucleotide composition, are the major factors governing metallopeptide site-selective DNA reactivity. For example, early on, we established that homopolymeric DNA sequences, such as polyA sites, while indeed A/T-rich but narrowed to an extent greater than canonical mixed A/T-rich regions, do not provide good substrates for metallopeptide cleavage.[14] Meanwhile, narrowed, noncanonical G/C sites, such as 5′-CCT, can provide suitable substrates for some metallopeptides.[14,27] These observations suggest that the wide minor groove of canonical G/C regions leads to a less efficient metallopeptide interaction, as typically observed with other minor groove binding agents.[28] Perhaps the width of the minor groove at mixed A/T regions and other minor groove nucleotide compositions that resemble this width are neither too wide nor too narrow, steering the metallopeptide catalyst in such a way as to optimize access to the C4′−H target; correct groove width may also serve to optimize residence time of the DNA-associated metallopeptide "catalyst", leading to a greater relative observed reactivity.

Along with explaining features inherent to the metallopeptide−minor groove interaction, the foregoing study serves to illustrate fundamental aspects of small molecule/peptide DNA recognition that impacts our understanding of drug−DNA interactions and design, in general. In particular, (1) the location of a positively charged moiety within a DNA-targeted structure is as influential as its presence or absence; (2) subtle steric differences between diastereomeric species can impact the structural complementarity of a ligand−DNA interaction, leading to altered DNA cleavage activities; and (3) the presence of guanidinium versus protonated amine functionalities, while driving a similar overall electrostatic interaction, can lead to different stabilities between low molecular weight DNA binding agents. The above points further demonstrate the viability of simple metallopeptides as conveniently altered models to discern details of low molecular weight agent−DNA interactions.

Experimental Section

Materials. Plasmid pBR322 was purchased from Invitrogen. All electrophoresis reagents (acrylamide, bisacrylamide, tris-base, boric acid, acetic acid, and EDTA) were purchased from Fisher Life Sciences. Radioisotopes were purchased from Perkin-Elmer ([α-^{32}P]dATP) and NEN ([γ-^{32}P]ATP). Enzymes were purchased from Invitrogen (EcoRI), Promega (RsaI and T4 kinase), Roche Molecular Biochemicals (terminal deoxynucleotidyl transferase), and Fisher (bacterial alkaline phosphatase). Microcon centrifugal concentrators were purchased from Fisher Life Sciences and used according to the manufacturer's protocols. Other reagents were purchased at the highest available purity from Sigma-Aldrich. All buffers were prepared using water from a Millipore Milli-Q water purification system. All peptides employed in this study were synthesized manually through standard Fmoc protocols using commercially available side-chain-protected amino acids from Bachem. Peptide purity was achieved and monitored using a Varian HPLC employing a Rainin reverse-phase C_{18} column; peptides were verified through ESI-MS analyses.

Restriction Fragment Cleavage Analyses. DNA restriction fragments employed as ^{32}P-end labeled substrates for metallopeptide-induced cleavage were isolated from pBR322 by restriction fragment digestion and other established protocols.[29] Typically, 25 μg aliquots of commercial plasmid were treated with Eco RI (1 h at 37 °C with 150 units of EcoRI in 50 mM Tris-HCl, pH 8.0/10 mM $MgCl_2$/100 mM NaCl buffer) and subsequently dephosphorylated through treatment with bacterial alkaline phosphatase (1.5 units) for 1 h at 65 °C. The DNA was 5′-end labeled by treating the above linearized plasmid with T4 polynucleotide kinase for 30 min at 37 °C in the presence of 100 μCi of [γ-^{32}P]ATP. Alternatively, the DNA was 3′-end labeled through treatment with terminal deoxynucleotidyl transferase and 100 μCi [α-^{32}P]ddATP. The resulting radiolabeled DNAs were further digested with RsaI for 1 h at 37 °C to yield ^{32}P-end labeled 167 and 514 base pair fragments that were purified by 6% preparative nondenaturing gel

(27) Sy, D.; Savoye, C.; Begusova, M.; Michalik, V.; Charlier, M.; Spotheim-Maurizot, M. *Int. J. Radiat. Biol.* **1997**, *72*, 147−155.
(28) Neidle, S. *Nat. Prod. Rep*. **2001**, *18*, 291−309.
(29) Maniatis, T.; Fritsch, E. F.; Sambrook, J. *Molecular Cloning*; Cold Spring Harbor Laboratory: New York, 1982.

electrophoresis. Bands containing radiolabeled material were visualized by autoradiography, excised, and isolated through crushing and soaking.

Metallopeptide-induced cleavage reactions were carried out in 10 μL total volumes containing 50 μM (base pair) sonicated calf thymus DNA carrier and 1×10^4 cpm of a radiolabeled restriction fragment in 10 mM cacodylate buffer, pH 7.5. Reactions were initiated through admixture of DNA and preformed $Ni(OAc)_2$ + peptide in 50 mM cacodylate buffer, pH 7.5. For metal-free and peptide-free controls, the eliminated reagent was replaced by an equivalent volume aliquot of deionized water. After a 10 min incubation of DNA + metallopeptide at room temperature, 2 μL aliquots of $KHSO_5$ in water were added to the DNA + metallopeptide mixture to complete the final reaction volume of 10 μL and to bring all components to their final concentrations (see figure legends). Reactions were allowed to proceed for 1 min and were subsequently quenched through the addition of 2 μL of a 0.2 mM EDTA solution, EtOH-precipitated, and dried. The resulting DNA pellets were dry-counted to normalize counts for gel loading and redissolved in 1.5 μL of an 80% formamide loading buffer. Equivalent counts of each reaction mixture, along with A+G and/or T+C Maxam−Gilbert standard reactions,[29] were heat denatured at 90 °C for 5 min and quick-chilled on ice. The samples were loaded onto 12 or 15% 19:1 polyacrylamide/7.5 M urea sequencing gels which had been prerun to a temperature of 50 °C. Gels were electrophoresed (1500 V for ~8 h) in TBE buffer. Gels were removed, transferred to an autoradiography cassette, and exposed (wet) to film (Kodak X-omat) at −70 °C.

Molecular Modeling and Simulations. All calculations were performed with the following software packages: SPARTAN 5.1,[30] MacroModel 7.0,[31] and AMBER 7.[32] Default settings for these programs were used unless specified otherwise. The coordination complexes described in this paper are based on a crystal structure[25] of Gly-Gly-His bound to Ni^{2+}; missing force field parameters were developed for this basic ring system as described.[17]

Assembly of each metallopeptide−DNA complex was carried out in the following general manner. Beginning with the atomic coordinates of netropsin-bound $d(CGCGAATTCGCG)_2$ or $d(CGCGTTAACGCG)_2$ from the PDB (reference codes 1D86 and 195D, respectively), the netropsin molecule was deleted from the minor groove, and the metallopeptides (containing appropriate side chain substitutions) were inserted manually at the dyad axis of the oligonucleotide substrate with the translation/rotation facility of MacroModel. Each metallopeptide was docked with its amino-terminal amine and imidazole edge inserted into the minor groove. The docked starting structures produced for each metallopeptide were generated independent of the 1D and 2D NMR studies performed earlier[17] (i.e., constraints based on observed NOEs were not used in the generation of these starting structures nor were any constraints employed during the course of the modeling and simulations that could potentially bias the results); however, the distance between the His imidazole C4 proton and the A_6 C2H of the AATT oligonucleotide was approximately 4−5 Å for each metallopeptide studied, suggesting a close correspondence to the NMR-derived structures for these metallopeptides.[17] Bump-checking was turned on to ensure no overlapping atoms resulted during the docking process, and these initial minor groove-bound DNA complexes were exported to AMBER. To these complexes were added the requisite number of Na^+ counterions by standard procedures to achieve electroneutrality of the 11 phosphate anions provided by each single strand of DNA (21 or 22 counterions were added, in the presence of a positively charged or charge-neutral metallopeptide, respectively) using the addIons command in the XLEaP facility of AMBER. Subsequently, the complex was solvated explicitly using the TIP3P water potential inside a central simulation box. The box dimensions ensured solvation extended 10 Å on all sides of the DNA−metallopeptide complex. The dimensions, number of waters, and corresponding Γ values for each system studied are given in Supporting Information.

The protocol for all MD simulations described herein included the following procedure. First, the docked metallopeptide−DNA complex, with associated Na^+ ions and water bath, were energy minimized with 500 steps of conjugate gradient minimizer using 100 kcal $(mol\cdot Å)^{-1}$ restraints on DNA and counterion positions. Subsequently, during three 500-step minimizations, the restraints were relaxed stepwise by 25 kcal $(mol\cdot Å)^{-1}$ per step. Following the above steps, a fifth 500-step minimization was performed without restraints. Next, the optimized structure achieved was heated from 100 to 300 K over a time period of 25 ps with a temperature coupling of 0.2 ps while using positional restraints of 100 kcal $(mol\cdot Å)^{-1}$ for the DNA complex and its associated counterions. A constant volume was maintained during this process. Following the above, there were four sequential 15 ps MD steps at 300 K with a gradual loosening of restraints of 25 kcal $(mol\cdot Å)^{-1}$ per step. Finally, the system without restraints was allowed to equilibrate for an additional 15 ps; the temperature was allowed to fluctuate around 300 K with a temperature coupling time of 0.2 ps, and the pressure was allowed to fluctuate around 1 bar with a pressure coupling of 0.2 ps. Production runs in excess of 1400 ps were carried out following this protocol. Upon energy minimization, thermal warming, and molecular dynamics (MD) equilibration of each solvated starting structure, the energy of each system was observed to be stable for the remainder of its respective simulation. For each system studied, the root-mean-squared (RMS) deviation of the DNA + metallopeptide complex, the DNA alone, and the metallopeptide alone with respect to their starting structures attained equilibrium after 250 ps. Hence a time period 500 ps after thermal warm-up was selected as a starting point for data collection for these simulations. For each simulation, 5000 structures were saved to disk for postprocessing by uniformly sampling the trajectory during the production run. All analyses of results were done using the CARNAL and ANAL programs in AMBER.

Acknowledgment. We thank the National Institutes of Health for financial support of this work (GM 62831 to E.C.L.). In addition, Y.F. would like to acknowledge funding from the National Institutes of Health (G12 RR003048 from the RCMI program, Division of Research Infrastructure, National Center for Research Resources through Howard University) for support during the preparation of this publication.

Supporting Information Available: Details of MD simulations, including metallopeptide + oligonucleotide starting structures and average structures, and complete ref 32. This material is available free of charge via the Internet at http://pubs.acs.org.

JA0569757

(30) Kanemasa, S.; Oderaotashi, Y.; Yamamoto, H.; Tanaka, J.; Wada, E. *Spartan*; Wavefunction, Inc., 18401 Von Karman, Suite 370, Irvine, CA 92715.
(31) Mohamadi, F.; Richardson, N. G. J.; Guida, W. C.; Liskamp, R.; Lipton, M.; Caufield, C.; Chang, G.; Hendrickson, T.; Still, W. C. *J. Comput. Chem.* **1990**, *11*, 440−467.
(32) Case, D. A.; et al. *AMBER 7*; University of California, San Francisco, 2002.